

Conf-800205--18

THE USE OF SMALL-ANGLE X-RAY AND NEUTRON SCATTERING FOR CHARACTERIZING

VOIDS IN NEUTRON-IRRADIATED METALS AND ALLOYS*

CONF-800205--18

Robert W. Hendricks
Technology for Energy Corporation
Knoxville, Tennessee 37922

DE83 007510

Small-angle x-ray and neutron scattering are powerful analytical tools for investigating long-range fluctuations in electron (x-rays) or magnetic moment (neutrons) densities in materials. In recent years they have yielded valuable information about voids, void size distributions, and swelling in aluminum, aluminum alloys, copper, molybdenum, nickel, nickel-aluminum, niobium and niobium alloys, stainless steels, graphite and silicon carbide. In the case of aluminum information concerning the shape of the voids and the ratio of specific surface energies was obtained. The technique of small-angle scattering and its application to the study of voids is reviewed in the paper. Emphasis is placed on the conditions which limit the applicability of the technique, on the interpretation of the data, and on a comparison of the results obtained with companion techniques such as transmission electron microscopy and bulk density.

DISCLAIMER

This report was prepared as an account of work sponsored by an agency of the United States Government. Neither the United States Government nor any agency thereof, nor any of their employees, makes any warranty, express or implied, or assumes any legal liability or responsibility for the accuracy, completeness, or usefulness of any information, apparatus, product, or process disclosed, or represents that its use would not infringe privately owned rights. Reference herein to any specific commercial product, process, or service by trade name, trademark, manufacturer, or otherwise does not necessarily constitute or imply its endorsement, recommendation, or favoring by the United States Government or any agency thereof. The views and opinions of authors expressed herein do not necessarily state or reflect those of the United States Government or any agency thereof.

DISTRIBUTION OF THIS DOCUMENT IS UNLIMITED

*This research was performed while the author was a Senior Staff Member of the Metals and Ceramics Division, Oak Ridge National Laboratory, Oak Ridge, Tennessee 37830, and was sponsored by the Division of Materials Sciences, U.S. Department of Energy, under contract W-7405-eng-26 with the Union Carbide Corporation.

MASTER

By acceptance of this article, the publisher or recipient acknowledges the U.S. Government's right to retain a nonexclusive, royalty-free license in and to any copyright covering the article.

Handwritten signature

Introduction to Small-Angle Scattering

As with all scattering techniques, the amplitude of x-ray or neutron scattering is related to the scattering length density (electron density for x-rays; coherent nuclear scattering length density or magnetic moment density for neutrons) by a Fourier transform. Thus, the characteristic angle at which radiation is scattered and the size of the scattering object are inversely related. Typically, x-ray wavelengths are in the range 0.5-2.0 Å while neutron wavelengths are 1-15 Å. The scattering objects of interest in small-angle x-ray scattering (SAXS) or small-angle neutron scattering (SANS) are typically 10-10 000 Å. Because the object dimensions are large compared to the wavelength of the incident beam, the resultant scattering occurs in the very small angular region of 0.005-5°. In order that measurements can be made at such small angles, special collimation techniques have been developed during the past 40 years. It is these specialized collimation techniques which have separated the field of small-angle scattering from the more classical fields of high-angle x-ray and neutron diffraction.

What information can be obtained from small-angle scattering? The scattering intensity for a single particle is given by

$$I(\underline{k}) = \sum_m \sum_n f_m f_n e^{i\underline{k} \cdot \underline{r}_{mn}} , \quad (1)$$

where

f_m = the scattering amplitude of the m^{th} atom,
 \underline{r}_{mn} = the vector separation of the m and n^{th} atoms, and
 \underline{k} = the diffraction vector.

This expression, given generally for x-ray scattering, is appropriate to neutron scattering when there are no inelastic neutron scattering effects. The magnitude of the diffraction vector is given by

$$|k| = \frac{4\pi}{\lambda} \sin\theta , \quad (2)$$

where

λ = radiation wavelength, and
 2θ = the scattering angle.

In the case of N randomly oriented, independently scattering, centrosymmetric particles it can be shown that at small scattering angles (1)

$$I(k) = NV^2 \Delta\rho^2 \int_0^\infty \gamma(r) \frac{\sin kr}{kr} 4\pi r^2 dr , \quad (3)$$

where

$\gamma(r)$ = characteristic function of the particle,
 $\Delta\rho$ = difference in scattering length of the particle and its matrix,
and
 V = volume of the particle.

The characteristic function has been computed for a variety of randomly oriented particles of various shapes (1).

Although the exact shape of the scattering curve depends on the shape of the scattering particles, there are several general results which are independent of the shape (1).

I. At $k = 0$

$$I(0) = NV^2 \Delta\rho^2 . \quad (4)$$

II. At small values of k , $\frac{\sin kr}{kr}$ can be expanded as a series which leads to (1)

$$I(k) = I(0)e^{-k^2 R_g^2/3} , \quad (5)$$

where

R_g is the radius of gyration of the particle. Equation (5) is known as Guinier's law.

III. At large values of k , an approximate expression for the intensity can be obtained by expanding the characteristic function $\gamma(r)$ about small values of r (1). The leading term of the result shows

$$I(k) = \frac{2\pi \Delta\rho^2 S}{k^4} , \quad (6)$$

where S is the total interphase surface area. Equation (6) is known as Porod's law.

IV. A Fourier inversion of Eq. (3), evaluated at $r = 0$, yields

$$Q_0 \equiv 4\pi \int_0^\infty k^2 I(k) dk = 8\pi^3 \Delta\rho^2 NV . \quad (7)$$

The left-hand side of Eq. (7) is defined as the invariant and is denoted by Q_0 . The invariant is quickly recognized to be the total scattered intensity integrated over all space.

V. Finally, if the particles are spherical in shape, the characteristic function is easily evaluated, and we find

$$I(k) = NV^2 \Delta\rho^2 \frac{9\pi}{2} \frac{J_{3/2}^2(kR)}{(kR)^3} , \quad (8)$$

where $J_{3/2}(x)$ is a Bessel function, and R is the sphere radius.

If there is a distribution of sphere sizes, then

$$I(k) = \int_0^\infty N(R) I(k,R) dR / \int_0^\infty N(R) dR , \quad (9)$$

where $I(k,R)$ is given by Eq. (8) and $N(R)$ is number of particles with radii between R and $R + dR$. It is important to note that $I(k,R)$ is weighted by the square of the volume of the particle. Thus, the forward scattering from a 100 Å diameter particle (void) is 10^6 greater than that from a 10 Å diameter particle. A variety of techniques have been developed to unfold the integral equation of Eq. (9) to recover $N(R)$ under the assumption that the individual particles are spheres and obey the scattering equation of Eq. (8) (2).

Each of these results has been used in the study of voids in irradiated metals and alloys, as will be described in a later section of this review.

Small-Angle Scattering Instruments

In order to measure scattering at the small angles described in the previous section, the incident beam must be collimated very finely. In the early days, such collimation reduced the power of the incident beam such that the diffusely scattered radiation could not be observed over the noise of the detector (i.e., fog with film, and cosmic and electronic noise for photon counting detectors such as proportional or scintillation detectors). The early compromise for SAXS was to collimate the beam very well in one direction, but only very poorly in the orthogonal direction. This led to numerous camera geometries such as the Kratky, Guinier, or Beeman four-slit, all of which are in use today. Such cameras have been very practical for the study of macromolecules in solution, but have serious limitations for metallurgical work. First, the beam size is fairly large (approximately 0.060 by 30 mm), thus requiring large, thin samples. More importantly, the large angular divergence of the incident beam in the long direction (typically $\pm 20^\circ$) led to serious problems with a form of multiple scattering known as double-Bragg scattering. Only in those cases involving large, thin metal foils with very high scattering power (e.g., GP zones in Al-Zn) could such instruments be used effectively. With considerable effort, Epperson et al. (3) irradiated large aluminum single crystals and studied the small-angle scattering from the radiation induced voids using a Kratky camera. To solve the problem of thinning such large samples to the optimum thickness for the transmission of x-rays [$t_{\text{opt}} = 1/\mu$, where μ is the linear absorption coefficient] $\text{AgK}\alpha$ ($\lambda = 0.5 \text{ \AA}$) was used. These results will be discussed in the next section.

Because neutron beams and sample sizes are typically measured in centimeters rather than millimeters, long-slit neutron machines were never practical. It was not until the advent of position-sensitive detectors (PSDs) that point-geometry small-angle collimation systems became possible. With position-sensitive detectors the electronic and cosmic noise is distributed over numerous counting channels; 10^2 for a linear detector, 10^3 - 10^5 for an area detector. Thus, the background was decreased from 0.1 to 1 cps for a non-position-sensitive counter to 10^{-3} - 10^{-2} cps/channel for a PSD. This enormous increase in sensitivity thus made it possible to work with the significantly decreased incident beam intensity available in point collimation. The first SANS facility, with an array of six linear PSDs, was constructed in Jülich by Schelten (4), and was followed by the big D-11 facility developed at the Institute Laue-Langevin in Grenoble by Ibel (5). The enormous success of these machines spurred the development of many more SANS facilities throughout the world (6-13). In the United States, facilities at the University of Missouri (6), the National Bureau of Standards (14), and Oak Ridge National Laboratory (11,12) are now operational and have appropriate geometries for metallurgical research. Of these, the NSF-funded user-dedicated 30-m facility at ORNL (11) promises to be one of the world's premier machines.

Following the development of successful point collimation SANS facilities using position-sensitive detectors, Schelten and Hendricks (15) constructed the first pinhole SAXS facility by fitting a Keissig film camera with an extended flight path and a linear PSD. They were able to show that the old problem of double-Bragg scattering, especially with polycrystalline foils, was caused principally by the wide divergence of the incident beam in the classical long-slit machines, and that with point collimation the problem was essentially eliminated even for 1.54 Å x-rays. With this instrument as

a highly successful prototype, Hendricks (16) developed the first x-ray facility which was equipped with an area detector. This machine utilizes a 6-kW rotating anode x-ray source, graphite monochromatization of the incident radiation, pinhole collimators separated by distances of up to 5 m, sample-to-detector distances of up to 5 m, and a two-dimensional position-sensitive proportional counter. It was designed especially for use with small (2.5 mm diam) metallurgical samples.

The field of small-angle scattering has literally exploded as a result of the application of position-sensitive detectors. The recent developments in instrumentation, theory and data analysis have been reviewed by Schelten and Hendricks (2), while Gerold and Kostorz (17) have reviewed the application of the technique to materials science. The special issue of the Journal of Applied Crystallography which contains these reviews is the proceedings of an international conference on the subject; the interested reader will find numerous papers which exemplify the applicability of small-angle scattering to a wide range of materials.

SAS Studies of Voids in Neutron-Irradiated Metals and Alloys

Small-angle x-ray and neutron scattering have been used to study voids in a wide variety of pure metals, alloys, semiconductors and insulators. Some of the published work is given in Table I. It is clear that the technique has been used extensively. However, it is not the purpose of this paper to review each of these investigations in detail. Rather, selected results from the literature will be used to illustrate the various kinds of information which can be obtained about voids and to emphasize the strengths and limitations of the technique for obtaining such information. The reader should keep firmly in mind throughout this discussion that it may not necessarily be possible to obtain all of the various types of information from any given sample or material.

Table I. Materials Investigated by Small-Angle Scattering

Type of Radiation	SAXS	References	SANS	References
Neutron Irradiated	Al	3,15,18,19	Al	20,21,22
	Mo	23,24	Cu	25,26
	Ni	16,27	GaAs	28
	SiC	29	Nb(Zr)	30
	SiO ₂	31	NiAl	32
	Graphite	33,34	Stainless steel	8,30,35
Heavy Ion Irradiated	Nb	36		
	Ni	37		

It is seen from Eq. (3) and the subsequent results that the scattered intensity depends linearly on the number of defects (N), the square of the scattering length density difference between the defect and the matrix ($\Delta\rho^2$) and the square of the defect volume V^2 . Thus, any defect which has a scattering length density different from that of the matrix will scatter x-rays or neutrons at small angles. If multiple defects are present in the sample simultaneously, the observed scattering curve will be the weighted average from all the defects and the interpretation of the scattering curve can become quite complex. For the purposes of this discussion, the major defects which may present significant small-angle scattering are voids, small precipitate particles, and high densities of small dislocation loops.

It is thus implicitly assumed in the interpretation of most small-angle scattering data that only one type of defect is present in the sample. Such assumptions have proven to be generally valid in most of the research cited in Table I.

A typical small-angle x-ray scattering curve from voids in a sample of neutron-irradiated aluminum is shown in Figure 1. This pattern was obtained from a disc 3 mm in diameter and 74 μm thick in about 60 min measuring time on the pinhole camera described by Schelten and Hendricks (15). Similar data can now be obtained on the ORNL 10-m facility (16) in 1-2 min and, with an appropriately larger sample (2 cm diam by 1/2-2 cm thick) in a similarly short time on most major SANS facilities. From an analysis of the data of Figure 1, one can obtain the void radius of gyration [Figure 1(b) and Eq. (5)], and the void specific surface [Eq. (6)]. These results are given in Table II and are compared there with results obtained on a similar sample by SANS (ref. 21). The agreement of the results is excellent.

It is important to note that although the sample required for the SANS experiment is significantly larger than that required for SAXS, the SANS experiment is nondestructive and so the samples can be used for other tests (i.e., mechanical properties).

The radius of gyration can often be measured with great accuracy (1%). This is illustrated especially well by data obtained by Hendricks et al. (21) on a series of aluminum single crystals which were irradiated together under seemingly identical conditions along the axis of the RB-7 position of the beryllium reflector of the Oak Ridge High Flux Isotope Reactor (HFIR). The results are shown in Figure 2. The increasing trend in R_g was interpreted to result from an estimated 10°C increase in the reactor cooling water as it flowed from the top of the core to the bottom. Data of such accuracy result because SAS measures a bulk average over a very large number of voids ($\sim 10^{14}$), an averaging process which obviously cannot be obtained by other techniques.

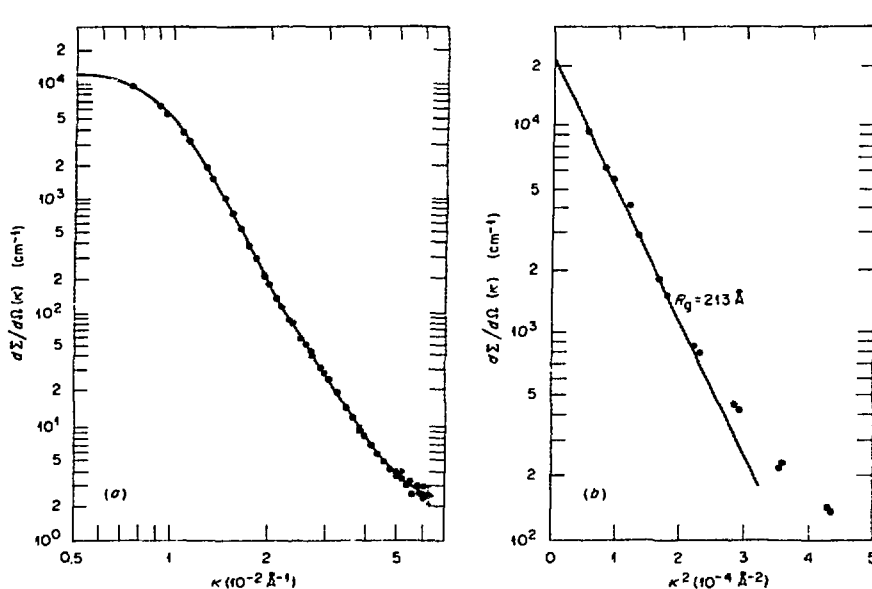


Figure 1. Small angle x-ray scattering from voids in a neutron-irradiated aluminum single crystal (fluence = $2.0 \times 10^{22} \text{ n cm}^{-2}$, $E > 0.18 \text{ MeV}$). (a) Scattering function recorded in a single run; (b) Guinier plot of innermost points (from ref. 15).

Table II. Comparison of the Small-Angle X-Ray Scattering Results for Specimen Al-6 with the Neutron Small-Angle Scattering Results for Specimen Al-5

Property	X-Rays	Neutrons
$d\Sigma(0)/d\Omega$, forward scattering*	$(2.7 \pm 0.2) \times 10^4 \times (NZr_T)^2$	$(2.60 \pm 0.05) \times 10^4 (Nb_{\text{coh}})^2$
R_g , radius of gyration (Å)	213 ± 10	215 ± 4
$\Delta V/V$, specific void volume swelling, %	0.72 ± 0.08	0.78 ± 0.04
S/V , specific void surface ($\text{m}^2 \text{cm}^{-3}$)	1.4 ± 0.3	1.3 ± 0.1

* N = number density of Al atoms = $6.06 \times 10^{22} \text{ cm}^{-3}$; Z = number of electrons per Al atom = 13; r_T = scattering amplitude of a classical electron = 2.82×10^{-13} , and b_{coh} = nuclear coherent scattering amplitude of Al = $3.441 \times 10^{-13} \text{ cm}$.

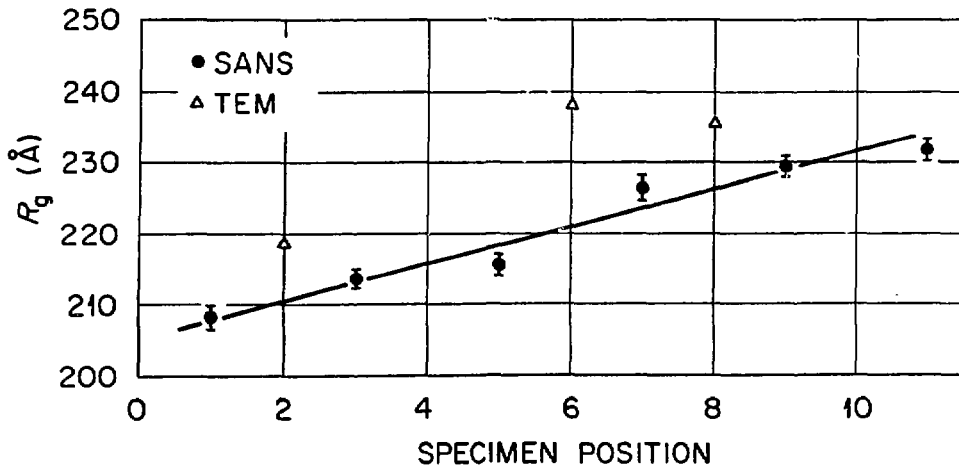


Figure 2. Radius of gyration R_g versus reactor core position (as identified by sample position - Position 1 is at the top, 11 at the bottom) (see ref. 21).

The swelling and specific surface of voids in the same series of neutron-irradiated aluminum single crystals are shown in Figure 3 and are compared with similar results from immersion density and transmission electron microscopy (TEM) measurements. It is seen that the SANS, TEM, and density measurements are in quite good agreement for the swelling; but that SANS and TEM do not agree well for the specific surface. This illustrates a particular strength of the small-angle scattering technique. In the derivation of Eq. (6), from which the results of Figure 3(b) are computed, there are no assumptions concerning the shape or size distribution of the voids. However, in obtaining a specific surface from TEM micrographs the image of a non-spherical (faceted) three-dimensional object is projected on a plane

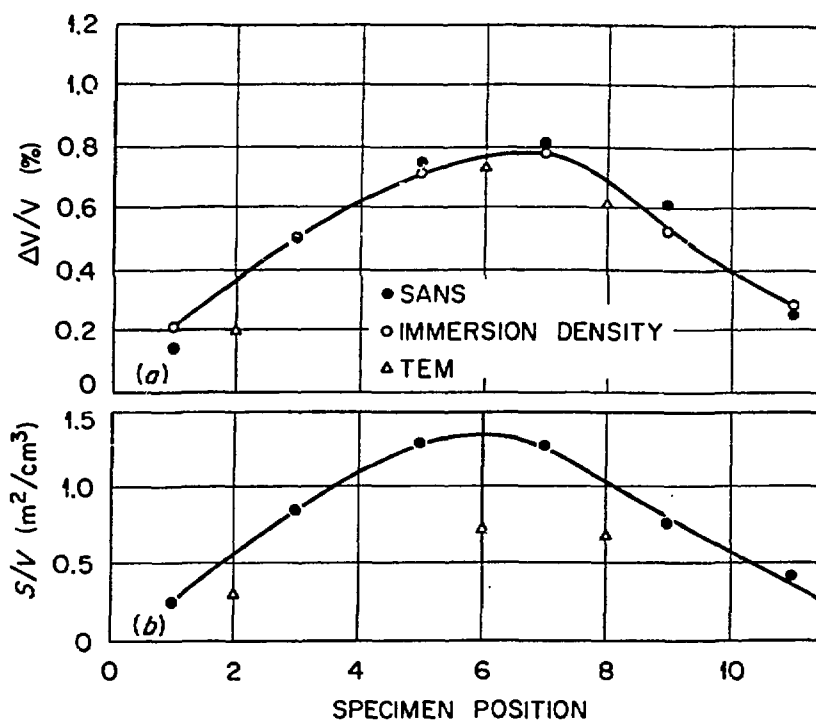


Figure 3(a). Swelling ($\Delta V/V$) versus sample position, and (b) total void surface area per unit volume of sample versus sample position as determined by SANS, TEM, and immersion density (from ref. 21).

(micrograph) whose size is characterized by a circle of radius R from which S/V is computed. Clearly, such procedures can lead to large errors, as is illustrated in Figure 3(b).

If the voids are assumed to be spherical (an assumption to be considered in the next section) then data such as shown in Figure 1 can be unfolded via Eq. (9) with the help of some very sophisticated computer codes to obtain an estimate of the void size distribution. A typical result for voids in neutron-irradiated aluminum are shown in Figure 4 along with TEM data from a companion sample. The results are generally in quite good agreement considering the assumptions and approximations involved in deriving both the TEM and SANS curves.

What appears to be the most significant observation is that all of the information presented in Table II and Figures 3 and 4 [radius of gyration, R_g ; swelling, $\Delta V/V$; specific surface, S/V ; and size distribution $N(R)$] can be obtained from an analysis of a single scattering curve which can be obtained in a few minutes. At the major small-angle scattering facilities, such as the National Center for Small-Angle Scattering Research in Oak Ridge, the necessary computer programs for such analysis have been developed and are readily available.

SAXS Studies of Voids in Metals Bombarded with Heavy Ions

The use of heavy-ion bombardment to simulate neutron irradiation of metals is of critical importance in reducing the time required to reach a given level of damage as compared to neutron irradiation, and special accelerator facilities have been developed for sophisticated multibeam (heavy ions plus hydrogen or helium) experiments (38,39). The characterization of voids and other defect structures in samples produced in such

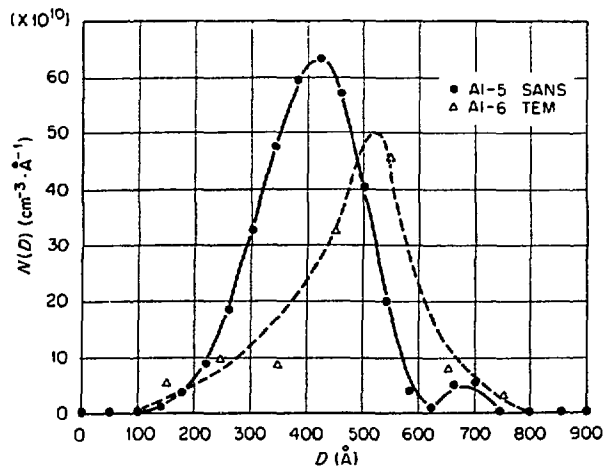


Figure 4. Size distribution for voids in Al-5 as compared with the TEM data of Al-6 (from ref. 21).

facilities poses special problems because the damage layer is very thin (generally less than 1 μm) and very near the specimen surface. Further complications arise because the void sizes are nonuniformly distributed within this damage layer. Considerable skill has been exhibited in developing thinning techniques to examine voids and defects in such samples by TEM.

Because the irradiated volume is so small, small-angle neutron scattering experiments are not possible with heavy-ion bombarded samples. However, a preliminary investigation on a nickel sample damaged to 9 dpa indicated that void sizes could be measured by small-angle x-ray scattering (37). In this experiment, a damaged nickel disc 3 mm in diameter was jet polished from the back via standard TEM preparation techniques to a thickness of 10 μm . The thinned region was about 1.5 mm in diameter and by careful control of the polishing conditions the dimple could be produced with a flat bottom. With such a sample, background scattering from defects other than voids comes from the entire 10 μm thickness while the desired signal, scattering from voids, comes only from the 1 μm layer. If we recall that the optimum thickness for the maximum scattered signal in a transmission experiment is $t_{\text{opt}} = \mu^{-1}$ where μ is the linear absorption coefficient, then for nickel studied with $\text{CuK}\alpha$ radiation, $t_{\text{opt}} = 27 \mu\text{m}$. Thus, in this experiment, the scattered intensity was roughly 30 times weaker than optimum and the signal-to-noise ratio was 10 times worse than normal. Nevertheless, a quite satisfactory SAXS pattern was obtained on the 10-m SAXS facility in under 1 h. The void sizes determined by SAXS were in good agreement with those obtained by TEM on similar samples. However, a further complication arises if one wishes to obtain the localized swelling $\Delta V/V$. The scattering experiment measures the total scattering from the independently scattering voids, but if the voids are nonuniformly distributed within the sample, as is the case here, there is no way to extract this information from the data. Thus, the local swelling cannot be determined by SAXS alone, but must have accurate theoretical (or experimental) damage distribution profiles.

Following this initial success, Epperson (36) has embarked on a detailed study of the role of oxygen in void formation in nickel-ion bombarded niobium. Here, niobium single crystals were doped with varying concentrations of oxygen and were then irradiated in the ORNL facility (38,39) at various temperatures and to several damage levels. Preliminary SAXS results from the 10-m facility are very encouraging.

Anisotropic Scattering Effects

It has been assumed in all of the preceding discussion that the voids, although not necessarily spherical in shape, were randomly distributed throughout the sample, both in orientation and spatially. Such is not necessarily the case, and two important deviations from these assumptions have yielded additional information from SAS measurements. The first to be discussed will be the effect of randomly distributed, oriented, faceted voids in a single crystal, and the second will be spatially ordered voids (the void lattice).

It has been well known from the first TEM observations that voids in metals are not spherical. Rather, they are faceted with the facet planes usually being low index crystallographic planes. Hendricks et al. (21) recognized that such faceting should produce an anisotropic scattering at higher k values in the small-angle scattering pattern. In the case of voids in neutron-irradiated aluminum, which are essentially octahedra bounded by $\{111\}$ planes, but which are also truncated on $\{100\}$ planes, they were able to calculate the structure factor. It showed a strong spherically symmetric central region surrounded by rods of diffuse intensity in $\langle 111 \rangle$ and $\langle 100 \rangle$ directions as depicted in Figure 5. Such patterns have been observed by Epperson et al. (3) with film techniques and by Spooner and Child (40) with a two-dimensional PSD. Analogous patterns for voids with other shapes have been observed in GaAs (28) and NiAl (32).

The calculations showed that at the higher k values the structure factor followed different asymptotic laws as shown in Table III. Thus, we see that although for randomly oriented voids the asymptotic law must average out to follow Porod's law [Eq. (6)], the asymptotic law for oriented voids may be very different in certain specific directions.

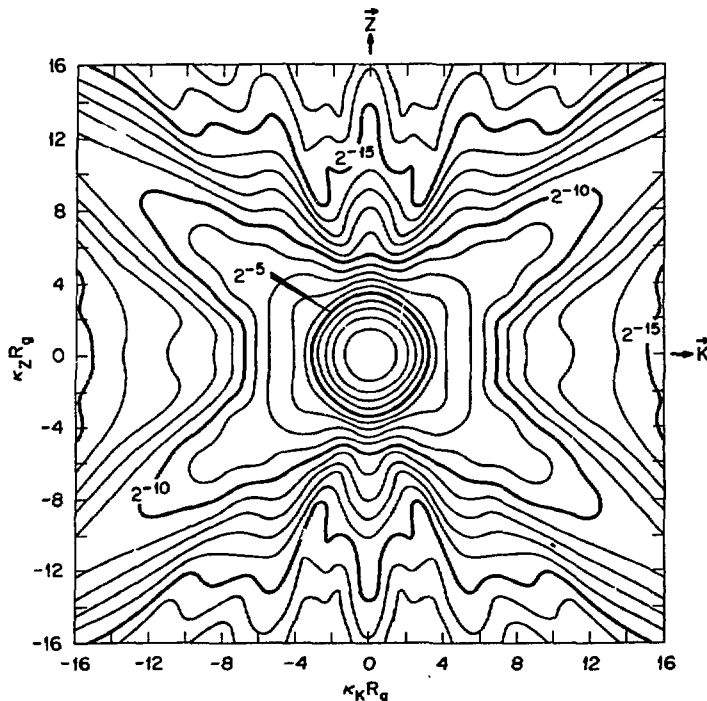


Figure 5. Calculated SAS pattern for truncated octahedral voids in Al. $[001]$ is vertical and $[110]$ is horizontal (from ref. 21).

Table III. Asymptotic Behavior of $|F_T(k)|^2$ for Untruncated Octahedra

$k \parallel$ to	Asymptotic Law
$\langle hkl \rangle$	$ k ^{-6}$
$\left. \begin{array}{l} \langle hk0 \rangle \\ \langle h00 \rangle \\ \langle hh0 \rangle \end{array} \right\}$	$ k ^{-4}$
$\langle hhh \rangle$	$ k ^{-2}$

$$h \neq k \neq l \neq 0$$

To test these ideas the scattering curves were measured at high angles in specific crystallographic directions as shown in Figure 6. Although the data fit the theoretical predictions in $\langle 111 \rangle$ directions with remarkable accuracy, it is seen that there is a considerable discrepancy between the anticipated result of k^{-4} in the $\langle 100 \rangle$ direction. This was attributed to the presence of a very small volume fraction of cubic voids which can be shown to have a k^{-2} dependence along $\langle 100 \rangle$. From these data it was estimated that the volume fraction of cubic voids was 0.18% of that of the octahedral voids. Since the volume fraction (swelling) of the latter was 0.8%, the volume fraction of cubic voids is 0.0014%! Such a small volume fraction of voids can be discerned because the cubic voids scatter most intensely in exactly the directions where the octahedral voids scatter weakly. These effects could certainly not be observed in polycrystalline samples where the scattering is smeared out into the Porod asymptotic average.

In their analysis of the structure factor which led to Figure 5, Hendricks et al. (21) found that at fixed lengths of the scattering vector (which corresponds to a circle drawn on Figure 5), the ratio of the intensity scattered in the $\langle 111 \rangle$ and $\langle 100 \rangle$ directions depended strongly on the degree

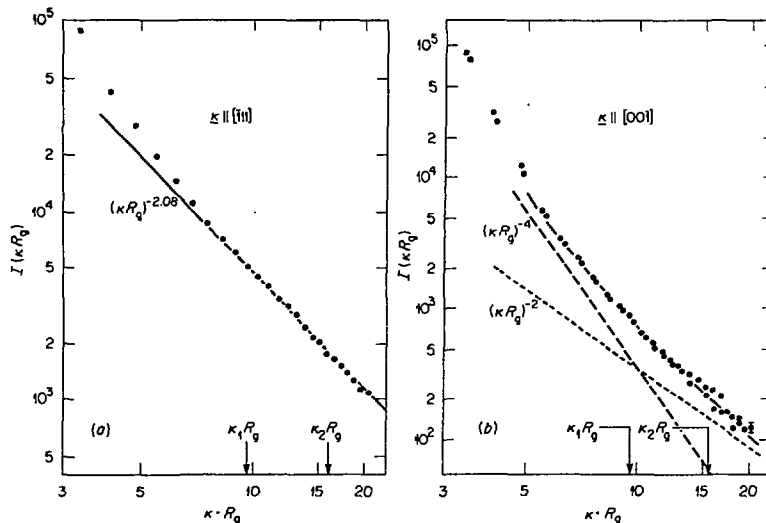


Figure 6. Scattered intensity along (a) $[111]$ and (b) $[001]$ for sample Al-5 as a function of HR_g . In (b) the void line is a fit of $C_2(kR_g)^{-2} + C_4(kR_g)^{-4}$. (From ref. 22).

This result was considerably higher than that expected for clean aluminum surfaces, and it was postulated that transmutation-produced Si contaminated the surfaces, thus preferentially changing the ratio. This hypothesis was later confirmed when Farrell et al. (41) observed a sheath of precipitated silicon on the surfaces of voids created in samples irradiated to significantly higher fluence than those examined by Hendricks et al.

Effects of Radioactivity

Metals and alloys which are irradiated to high fluences in nuclear reactors show varying degrees of radioactivity and varying half-lives for its decay. In the case of high-purity aluminum, the activity results mostly from ^{22}Na and decays rapidly. Thus, there is little difficulty in handling samples, even the very large ones used in the SANS experiments (20-22). Similarly, there were no significant problems associated with handling small molybdenum (23,24) or nickel samples (27). However, the high level of activity encountered by Schwann et al. (35) in their SANS investigation of stainless steel, and by Spooner in his SANS study of Nb(Zr) (30) required special techniques. In the case of niobium, the small disks used in SAXS experiments (3 mm ϕ and 100 μm thick) produced over 200 cps background in the area detector used in the 10-m SAXS facility at a distance of 5 m. This was ten times greater than the integrated scattering intensity from the voids in the sample. Even worse, the emitted radiation was MoK_{α} created by K-capture in niobium, and was indistinguishable from the incident MoK_{α} radiation used in the scattering experiment.

These results have shown that, although induced radioactivity may cause some problems and may preclude the use of either SAXS or SANS, usually one of the techniques can be used for the investigation of voids and void properties.

Summary

Small-angle and x-ray and neutron scattering, often in conjunction with transmission electron microscopy, have proven to be effective tools for obtaining the radius of gyration, size distribution, volume fraction, and specific surfaces of voids in a variety of neutron irradiated and heavy-ion damaged metals and alloys. In comparing the techniques, an important difference to be kept in mind is that TEM is the superior method for obtaining information on single and small numbers of defects, while SAXS and SANS are preferred when bulk averages over very large numbers of defects ($\sim 10^{14}$) are desired. The information on truncation parameters as obtained in the SANS rotation experiment on aluminum could be obtained by other means only with difficulty. In the author's experience, however, one should not emphasize one technique as compared to the other. Rather, SAXS, SANS, and TEM (along with other techniques such as positron annihilation and bulk density) should be viewed as complementary techniques, each providing a different and valuable kind of information in the study of voids. When a description of a void structure can be presented which is consistent with observations from several techniques, one has considerably more confidence in its validity.

References

1. A. Guinier and G. Fournet, Small-Angle Scattering of X-Rays, John Wiley and Sons, New York, 1956.
2. J. Schelten and R. W. Hendricks, J. Appl. Crystallogr. 11(5) (1978) 297-324.

3. J. E. Epperson, R. W. Hendricks, and K. Farrell, Phil. Mag. 30 (1974) 803-817.
4. J. Schelten, Kerntechnik 14 (1972) 86-87.
5. K. Ibel, J. Appl. Crystallogr. 9 (1976) 296-309.
6. R. M. Brugger, J. S. King, S. A. Werner, and W. B. Yelon, private communication, 1976.
7. C. P. Galotto, P. Pizzi, H. Walther, V. Angelastro, N. Cerullo, and G. Cherubini, Nucl. Instr. Methods 134 (1976) 369-378.
8. F. Frisius and M. Naraghi, Atomkernenergie 29 (1977) 139-144.
9. B. P. Schoenborn, J. Alberi, A. M. Saxena, and J. Fischer, J. Appl. Crystallogr. 11 (1978) 455-460.
10. C. Hofmeyer, R. M. Mayer, and D. L. Tillwick, J. Appl. Crystallogr. 12 (1979) 192-200.
11. W. C. Koehler and R. W. Hendricks, J. Appl. Phys. 50 (1979) 1951.
12. H. R. Child and S. Spooner, J. Appl. Crystallogr. 13 (1980) 259-264.
13. B. Farnoux, Les Spectrometres pour la diffusion aux petits angles Laboratoire Leon Brillouin, Report LLB/79/250/BF/MLC, 18 Dec. 1979; 91190 Gif-sur-Yvette, France.
14. C. J. Glinka, J. M. Roe, and J. G. LaRock, NBS Reactor: Summary of Activities July 1979 to June 1980, NBS Technical Note 1142, pp. 66-69 Washington, DC 20234. (May 1981).
15. J. Schelten and R. W. Hendricks, J. Appl. Crystallogr. 8 (1975) 421-429.
16. R. W. Hendricks, J. Appl. Crystallogr. 11 (1978) 15-30.
17. V. Gerold and G. Kostorz, J. Appl. Crystallogr. 11 (1978) 376-404.
18. V. W. Lindberg, J. D. McGervey, and W. Triftshausen, Phil. Mag. 36 (1977) 117-128.
19. J. D. McGervey, V. W. Lindberg, and R. W. Hendricks, J. Nucl. Mater. 69&70 (1978) 809-812.
20. H. A. Mook, J. Appl. Phys. 45 (1974) 43.
21. R. W. Hendricks, J. Schelten, and W. Schmatz, Phil. Mag. 30 (1974) 819-837.
22. R. W. Hendricks, J. Schelten, and G. Lippmann, Phil. Mag. 36 (1977) 907-921.
23. S. Liu, J. Moteff, J. S. Lin, and R. W. Hendricks, J. Appl. Cryst. 11 (1978) 597-602.
24. J. S. Lin, R. W. Hendricks, J. Bentley, and F. W. Wiffen (unpublished research).
25. C. Hofmeyer, K. Isbeck, and R. M. Mayer, J. Appl. Cryst. 8 (1975) 193.
26. C. Hofmeyer, R. M. Mayer, and E. T. Morris, Ann. Cont. S. Afr. Inst. Phys. (1976).
27. J. S. Lin and R. W. Hendricks (unpublished research).
28. S. Gupta, E.W.J. Mitchell, and R. J. Stewart, Phil. Mag. A 37 (1978) 227-243.
29. R. J. Lauf (private communication).
30. S. Spooner, this conference.
31. J. B. Bates, R. W. Hendricks, and L. B. Shaffer, J. Chem. Phys. 61 (1974) 4163-4176.
32. J. E. Epperson, K. W. Gerstenberg, D. Berner, G. Kostorz, and C. Ortiz, Phil. Mag. A 38 (1978) 529.
33. D. G. Martin and J. Caisley, Some Studies of the Effect of Irradiation on the Neutron SAS from Graphite, AERE-R-8515, Atomic Energy Research Establishment, Harwell, Great Britain.
34. P. Krautwasser (private communication).
35. D. Schwahn, D. Pachur, and J. Schelten, Neutron Scattering on Neutron Irradiated Steel, Report Jül-1543, October 1978, Kernforschungsanlage, Jülich GmbH, Jülich, West Germany.
36. J. E. Epperson (private communication).
37. R. W. Hendricks (unpublished research).
38. M. B. Lewis, N. H. Packan, G. F. Wells, and R. A. Buhl, Nucl. Instrum. Methods 167 (1980) 233.

39. N. H. Packan and R. A. Buhl, A Multispecimen Dual-Beam Irradiation Damage Chamber, Oak Ridge National Laboratory Report ORNL/TM-7276, Oak Ridge, Tennessee (June 1980).
40. S. Spooner and H. R. Child (private communication).
41. K. Farrell, J. Bentley, and D. N. Braski, Scripta Met. 11 (1977) 243.

11/15/77